Chapter 1

Introduction

A great deal of worldwide research efforts are directed towards the development of novel metallic, semiconducting and polymeric nanomaterials as solution dispersions for exploiting their vast potentials in several applications ranging from biology and medicine to environment and energy generation. Surprisingly, there is relatively less emphasis in literature on the development of reliable methods of surface immobilization of nanomaterials. There is an increasing realization in recent times that the surface confinement of nonmaterials on appropriate solid support will enormously enhance the application potentials of the materials. The challenge, however, lies in developing a suitable methodology to obtain stable and adherent deposits without jeopardizing their unique properties especially their catalytic activity. This thesis partly addresses this issue and focuses on the development of methods for surface immobilization of nanomaterials such gold nanoparticles, carbon nanotubes and biomaterials such as redox proteins. The nanomaterial coated surfaces have been characterized using different surface analytical methods and their electro catalytic activities have been validated by electrochemical techniques.

The first part of the thesis deals with the electrochemical synthesis of thiol stabilized gold nanoparticles, their *in situ* deposition onto the surfaces and their characterization using UV-vis spectroscopy, transmission electron microscopy, scanning electron microscopy and X-ray diffraction. The electrochemical properties of deposited Au NPs were studied using cyclic voltammetry and electrochemical impedance spectroscopy. The surface modified with gold nanoparticles (AuNPs) were studied for alcohol electro-oxidation reaction, glucose and dopamine sensing and finally as a hydrogen evolution catalyst.

The second part of the thesis deals with the surface immobilization of redox proteins and carbon nanotube functionalized proteins using the platform of self-assembled monolayers (SAM) of aromatic thiols on gold surface. Here, the surface confinement of the proteins has been demonstrated by the study of electron transfer and electrocatalytic properties using cyclic voltammetry (CV), and electrochemical impedance spectroscopy (EIS). The surfaces immobilized with protein and protein-SWNT composites were characterized using surface probe techniques such as atomic force microscopy (AFM) and scanning tunneling microscopy (STM).

While the major emphasis of the thesis is towards evolving a suitable methodology for surface confinement of nanomaterials and their characterization, there exists a considerable potential for developing several interesting applications. The present work, however, does not focus primarily on these applications. To that extent, the studies on the applications of the nanomaterials modified surfaces described in this thesis are by no means exhaustive. They are more illustrative in nature highlighting their potential, while a considerable scope exists for future work. This aspect has been briefly discussed at the end of the thesis.

The present chapter provides a general overview of different topics covered in this thesis. It begins with the general introduction to nanomaterials such as metal nanoparticles and carbon nanotubes, their synthesis, structure and properties. The next part describes the methods of formation self-assembled monolayers, immobilization of proteins on the SAM surfaces and a brief introduction to biosensors. The third and last part deals with a general description of the working principles of different experimental techniques used in the present thesis. These experimental techniques include cyclic voltammetry, electrochemical impedance spectroscopy, chronoamperometry, chronopotentiometry, X-ray diffraction, Fourier transform infrared spectroscopy, scanning electron microscopy, transmission electron microscopy and scanning probe technique such as atomic force microscopy and scanning tunneling microscopy.

1.1 Nanoparticles

Materials of nanoscale, typically in the range of 1-100 nm can be said to bridge the gap between small molecules and bulk materials. The metal nanoparticles, especially gold, silver and copper, have been extensively investigated over the past decade due to their unique electronic, optical and catalytic properties [1-4]. These properties are distinct from both bulk metal and molecular compounds demonstrated in both experimental and theoretical investigations. The properties strongly depend on the particle size, shape of the nanoparticles, and interparticle distance as well as the nature of the protecting organic shell [5]. The chemical stability of the particles is crucial to avoid degradation processes such as partial oxidation or undesired sintering of particles. The lack of sufficient stability of many nanoparticles has to some extent impeded the development of real world applications of nanomaterials.

Gold plays a special role as a material of choice in nanoscience and nanotechnology not just for its fascinating quantum physical properties, but more importantly for its versatile potential in several applications. Its importance arises due to its relative stability as colloidal

dispersion or even as dry particulate matter. Gold, both in the nanoscale and as a bulk material, also offers a fascinating surface chemistry that allows it to be used as a platform for the formation of self-assemble layers of organic thiol molecules. This is brought about by the unique affinity of gold to the sulfur atoms that has lead to several important and fundamental studies in electron transport through molecules, development of sensors and novel catalyst materials.

A catalyst is a substance which is added to a reaction but is not consumed during the process. Catalyst provides an alternative reaction pathway by decreasing the activation barriers of a reaction and hence, increasing the reaction rate [6]. Metal nanoparticles are promising catalyst materials for a variety of reactions, for example, oxidation, hydrogenation and C-C coupling reactions [7]. They have been explored as catalysts since the 19th century and later as industrial and petrochemical catalyst [8-10]. A major break through in nanoparticle catalysis came with Haruta's report that oxide-supported gold nanoparticles can be used as effective catalyst for low-temperature oxidations of H_2 and CO [11].

"Naked" metal nanoparticles are unstable and tend to aggregate, and even precipitate out of solution and lose their catalytic activities. Therefore, metal nanoparticles traditionally need to be supported on solid surfaces (*e.g.* oxide, carbon) to form heterogeneous catalysts [8]. The advantages of heterogeneous catalysts are that they are easy to separate from the reactants and products for recovery and reuse. They can also be used at high temperatures and pressures. They however suffer from poor catalytic activity and selectivity compared to many homogeneous catalysts [12]. An alternative method to stabilize metal nanoparticles is by using polymers, block copolymers, dendrimers, surfactants, or organic ligands as stabilizers [8]. Polymer or ligand stabilized metal nanoparticles can be uniformly dispersed in organic solvents or water and mixed with reactants and products in a way resembling a homogeneous catalytic system [13]. However, insufficient stability and high costs, due to difficulties in recovery and reuse, are major drawbacks [14]. The facile synthesis stable and solution processable thiol functionalized nanoparticles by the Brust method was an important milestone in the gold nanoparticles research [15,16]. This immediately provided a versatile tool for the attachment of several terminally functionalized thiols on the nanoparticles and also biomaterials including enzymes, proteins and nucleotides[17].

The following sections describe the common methods of synthesis, properties and application of nanoparticles:

1.1.1 Physical Methods

In the physical methods, the nanoparticles have been obtained by evaporation of a solid material to form a supersaturated vapor from which homogeneous nucleation of nanoparticles takes place. In these methods, the size of the particles is controlled by temporarily inactivating the source of evaporation, or slowing the rate by introducing gas molecules to collide with the particles. The general physical methods include inert gas condensation, arc discharge, ion sputtering, laser ablation, and pyrolysis.

1.1.2 Chemical Methods

The chemical methods are generally carried out at mild conditions and the synthesized nanoparticles are solution dispersible as sols. The formation of sols consists of three steps:

1) Seeding
2) Particle growth and
3) Growth termination by capping

The important process that occurs during growth of colloid is Ostwald ripening. This is a growth mechanism whereby smaller particles while dissolving release monomers or ions for consumption by larger particles, the driving force being the lower solubility of larger particles. Ostwald ripening limits the ultimate size distribution obtainable to about 15% of the particle diameter when the growth occurs under equilibrium conditions. The seeding, nucleation, and termination steps are not separable. The relative rates of these steps can be altered by changing parameters such as concentrations and temperature. The monodisperty of nanocrystals depend on the synthetic methods, choice of capping agent, concentration, and temperature. The gold nanoparticles are generally synthesized using a reducing agent along with the stabilizers. The popular methods of synthesis are described below

1.1.2.1 Borohydride Reduction Method

The basic reaction involved in the borohydride reduction proceeds via evolution of H_2;

$BH_4^- + 2H_2O \rightarrow BO_2^- + 4H_2$

Brust and Schiffrin developed a two phase method to reduce the noble metals. This method, has been widely used to synthesize nanoparticles [15-16]. In this method, aqueous metal ions are transferred to a toluene layer by tetraoctylammonium bromide, a phase transfer catalyst which is also capable of acting as a stabilizing agent. The Au complex is transferred to toluene and reacted with alkanethiols to form polymeric thiolates. Aqueous borohydride is

added to this mixture to bring about the reduction that is modulated by the interface of toluene and water. The thiol molecules serve as a capping agent. As a result, alkanethiolate-protected gold nanoparticles also called monolayer-protected clusters (MPC), were produced with tunable particle size between 1 and 10 nm depending on the ratio of the Au salt and the ligand (alkanethiol). Later on, Murray and coworkers explored novel routes to functionalize MPCs by ligand place exchange reactions [18]. Alkanethiolate MPCs can be repeatedly isolated from and redissolved in common organic solvents without irreversible aggregation or decomposition. The particles can also be kept in solid state under ambient conditions for long time without significant ageing effects.

1.1.2.2 Citrate Method

Hauser and Lynn first time explained the citrate route for preparation of Au hydrosols. The method involves the addition of chloroauric acid to a boiling solution of sodium citrate [19]. A wine red color develops at the onset of reduction. By varying the concentration ratios of chloroauric acid and sodium citrate, particles of varying diameters can be prepared. Turkevich proposed that the reaction involved the formation and subsequent reduction of dicarboxylate species [20].

1.1.2.3 Alcohol Reduction

Metal nanoparticles can be produced by chemical reduction of metal salts by alcohols. By making use of polymeric capping agents such as PVP, the growth of metal particles can be arrested and stabilized [21-23]. Figlarz and coworkers developed a method of reduction of metal salts with high boiling polyols such as ethylene glycol which serve as the reducing as well as the stabilizing agent [24].

1.1.3 Electrochemical Synthesis

The electrochemical method is refinement of classical electrorefining process. Reetz et al. pioneered the electrochemical synthesis of nanoparticles [25]. The electrochemical synthesis consist of oxidative dissolution of anode, migration of metal ions to the cathodes, reduction of ions to zero-valent state, formation of particles by nucleation and growth, arrest of growth by capping agents, and precipitation of particles. The advantage of electrochemical synthesis compared to the chemical method is the high purity with which particles can be obtained. The size of the nanoparticles could be tuned using electrochemical techniques by altering the

current density, the distance between the electrodes, reaction time, the temperature, and polarity of the solvent.

1.1.4 Properties of Au NPs

Gold nanoparticles may be considered as the oldest of all the colloids as they are reported to have been prepared in 4th century B. C. and were used for several medical applications in the past. The structure of the nanoparticles has been studied extensively in literature and it was shown that the smallest particles have 12 gold atoms surrounding another gold atom in a close packed arrangement that totally contains 13 atoms. In bigger nanoparticles, the subsequent layers of gold atoms are shown to contain $10n^2+2$ atoms where n is the layer number. Hence the second layer contains 42 atoms forming Au_{55} cluster, third layer contains 92 atoms forming Au_{147} cluster and so on.

The average number of atoms per nanoparticles can be calculated assuming that nanoparticles are in spherical shape and a uniform fcc crystalline structure using formula [26]

$N = \pi\rho D^3 N_A/6\ M$ where,

N = number atoms per nanoparticles

ρ = density of face centered cubic (fcc) gold = 19.3 g/cm^3

D = average diameter of nanoparticles

M = Atomic mass of gold

N_A = number of atoms per mole

1.1.4.1 Electronic Properties

The ability of bulk metals to conduct electrons is due to the availability of continuum of energy levels above E_F, at the Fermi level. When a metal is divided finely, the continuum of the electronic states breaks down and it becomes insulating. The discreteness of energy levels does not physically manifest themselves as long as the gap is less than the K_bT, the themal energy at temperature T. In the case of semiconductors, a reduction in the size of the system causes the energy levels at the band edge to become discrete, with interlevel spacings similar to metals. This effectively increases the band gap of the semiconductor [27]. Figure 1 shows the schematic representation of the electronic structure of the bulk gold and nano crystals.

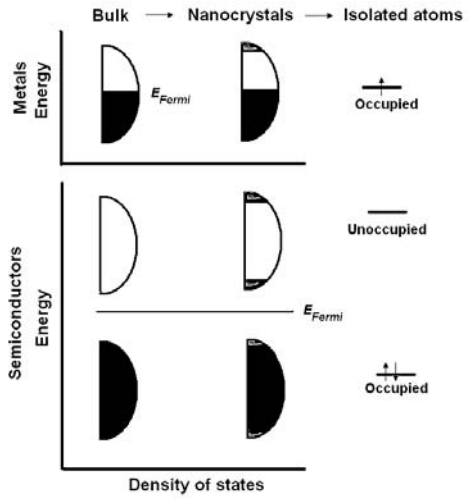

Figure 1. Schematic representation of the changes in the electronic structure accompanying a reduction in size, in metals and semiconductors [27].

1.1.4.2 Surface Plasmon Resonance of Au NPs

The properties of nanoparticles are different from that of bulk metals. This results from the quantum confinement of these particles, which arises when the de Broglie wavelength of the valance electrons are comparable to the size of the particles itself. Under such conditions the particles behave as electronically zero dimensional quantum dots. The freely mobile electrons are trapped in the clusters and show a characteristic collective oscillation frequency of the plasma resonance, giving rise to the so-called plasmon resonance band (PRB) or surface plasmon resonance (SPR) observed near 520 nm for the 3-20 nm diameter nanoparticles. In this range the phenomenon of size-dependent quantization occurs. The intensity of SPR band decreases with decreasing core size of Au NPs with 1.4-3.2 nm core diameters due to the onset of quantum size effects. This is important for particles with core size <3 nm in diameter, which also causes a small blue shift. It has been shown that the damping of the surface plasmon band varies inversely with radius due to surface scattering of the conduction electrons, which is accompanied by broadening of the plasmon bandwidth.

The surface plasmon band is absent for Au NPs with core diameter less than 2 nm, as well as for bulk gold. With elliptical particles, the band is shifted to higher wavelength as the spacing between particles is reduced, and this shift is well described as an exponential function of the distance between the two particles. The size-dependent confinement of the electrons results in the formation of selective energy levels by these standing electron waves. Such energy levels can be observed in scanning tunneling microscopy during the tunneling of electrons between tip and the nanoparticles which is known as the coulomb blockade. This

can be observed when the electrostatic energy $E_{el} = e^2/2C$ is more than the thermal energy (k_bT) where C is the capacitance of the nanoparticle. This shows that the coulomb blockade can be observed only when the capacitance is very low or the size of the particle is small. For nanoparticles with size about 5 nm, the capacitance is of the order of 10^{-18} F/cm^2 and hence the coulomb blockade can be visualized.

1.1.5 Applications of Au NPs

1.1.5.1 Biological Applications

Due to the unique properties of the nanoparticles and the easy functionalization with a variety of molecules using different functional terminal groups, they find diverse applications in the field of biosensors, catalysis etc. The review by Katz *et al.* has discussed in detail the different routes for enzyme or protein functionalization of nanoparticles [28]. The nanoparticles can be functionalized through electrostatic interactions between the stabilizer and the biomaterials. This is possible when the nanoparticles are stabilized by ionic groups like citrate or thiols with terminal ionic groups. With terminally functionalized thiols as stabilizers, like amino or carboxyl terminated thiols, the nanoparticles can be covalently attached with the biomaterials. Specific interactions can also be used for the functionalization if the Au NPs are stabilized using biomolecules like Lysine.

1.1.5.2 Electrochemical Studies

Viologen thiols have been used as redox-active linkers in order to study electron transfer between the linked GNPs [29]. Au NPs are also reported to be capable of tuning the electrochemical properties of the electrode/solution interface using the $[Fe(CN)_6]^{3-/4-}$ redox system [30].

1.1.5.3 Catalysis

Catalysis plays a vital role in providing fuels, fine chemicals, pharmaceuticals etc. The general feature of catalysis is that the catalytic reaction has a lower rate-limiting free energy change to the transition state than the corresponding uncatalyzed reaction, resulting in a larger reaction rate at the same temperature. This thesis mainly deals with the electrocatalysis of nanomaterials. Electrocatalysis is the process of enhancement of electrode kinetics by minimizing the overpotential which is a measure of departure of electrode potential from its equilibrium value. In other words overpotential is the extra potential over the equilibrium value that must be applied to cause an electrochemical reaction at a certain rate. An electrodic

reaction may be anodic (oxidation) or cathodic (reduction) depending upon the direction of overpotential with respect to the equilibrium potential of the electrode.

Gold nanoparticles are very good catalysts for a variety of reactions. For example they are excellent catalyst for the CO oxidation and a large number of studies have been reported in this field. The Au NPs are also shown to catalyze methanol and ethanol oxidation as well as oxygen reduction, which has immense industrial applications in the field of fuel cells. In direct methanol fuel cells (DMFCs) Pt has been used as a catalyst. However adsorption poisoning of the catalyst by reaction intermediates limits its use in application. In order to overcome poisoning effect of Pt, alloys of Pt, Au, Ru, Sn, etc., have been intensively studied for methanol oxidation reactions [31].

In this thesis, Au NPs modified surfaces have been characterized as anode for methanol and ethanol fuel cells application in alkaline medium.

1.2 Carbon Nanotubes

Carbon nanotubes are the tubular structures formed by the carbon atoms. They may be represented as the rolled hexagonal network of graphite sheets. There are mainly two types of carbon nanotubes namely single walled nanotubes (SWNTs) and multiwalled nanotubes (MWNTs). MWNTs are the one that was first reported in the literature by Ijima in 1991 [32]. In 1993, Ijima *et al.* and Bethune *et al.* simultaneously and independently reported the synthesis of SWNTs by a cobalt catalyzed reaction [33-34]. SWNTs are a single layer of tubular carbon with diameter from 1.2-10 nm, while MWNTs contains several concentric graphitic shells with a shell separation of ~0.35 nm and the diameter varies from few nanometers to several tens of nanometers. The length of the nanotubes may be up to a few microns, that depending on the the synthetic conditions [35]. A schematic model of SWNTs and MWNTs are represented in the Figure 2.

In the present thesis, we have used the SWNTs and the following discussion is on the brief synthesis, properties and applications of SWNTs.

1.2.1 Synthesis and Purification of SWNTs

Several methods have been proposed for the synthesis of SWNTs. Some of the most common methods are arc-discharge, chemical vapor deposition and laser ablation methods [36]. In the arc-discharge method, two graphite rods are used as sacrificial anode and cathode, separated by about 1-2 mm. Iron, nickel or cobalt metal is included as a catalyst which is essential for

the single walled nanotubes formation. A high DC of the order of 80-100 A under helium or argon atmosphere (~500 torr) is applied to the graphite electrodes. During the arcing, a deposit forms on the cathode that contains the nanotubes having diameter in the range of 0.75 nm to 13 nm. Large amount of SWNTs can be prepared with high yield (~80%) by this method using Ni-Co, Co-Y or Ni-Y catalyst filled in the anodic rod under helium atmosphere [37]. The chemical vapor deposition method is based on the chemical decomposition of carbon containing gases like ethylene or acetylene in the presence of a metal catalyst. A substrate modified with metals like iron, nickel or cobalt is heated to ~700 °C in a heating chamber. The carbon containing gas is passed into this chamber in the presence of nitrogen or hydrogen. The gas decomposes at the metal sites with the formation of nanotubes. In laser ablation method, high power laser vaporization of graphite take place using metal as catalysts under conditions of high temperature (~1200 °C) and inert atmosphere, producing SWNT bundles of diameter ~13nm [38].

As described above, metal particles are essential for the production of nanotubes. Metals like Fe, Ni, Co, Mn and Y have been commonly used as catalyst for the nanotubes production and these metal particles normally get into the nanotube bundles. Many residual carbon particles are also present in the nanotube bundles. Hence, extensive purification is needed for the nanotubes before studying their special properties. Acid treatment has been extensively used for the removal of metal particles from the nanotubes. It has been shown that refluxing the nanotube with conc. HNO_3 dissolves the metals as metal nitrates that can be filtered off from the nanotubes easily. This also results in the acidification of the nanotubes with carboxyl functionalization at the terminal carbons. In our experiments, the purification was carried out by an acid refluxing method with 6N HNO_3 [39]. The Ni concentration, which is the main impurity in the nanotubes prepared by arc-discharge method, in the raw SWNTs was 17.5% while in the purified nanotubes it was only 0.234% indicating the high efficiency of the purification. Another major impurity in the nanotubes is the residual carbon particles which can be easily removed by heating the nanotubes at high temperatures. We have heated the nanotubes to about 350 °C for the removal of all non-tubular carbon forms present in the nanotubes sample.

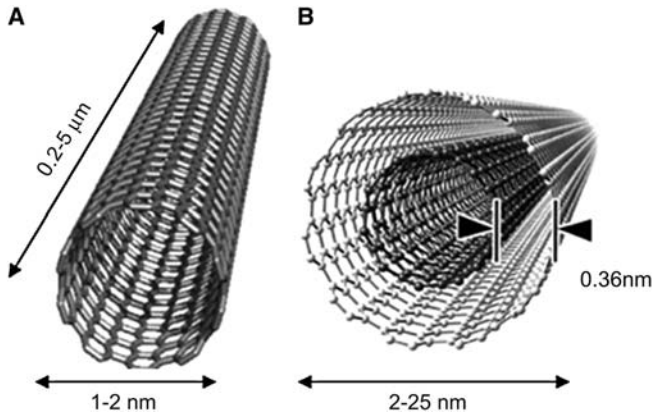

Figure 2. Schematic representation (A) SWNT and (B) MWNT.

1.2.2 Structure and Properties of Nanotubes

The SWNTs are classified as three types, based on the structure as armchair, zig-zag and chiral nanotubes. As the name indicates, the terminal carbon atoms in armchair nanotubes forms a structure similar to the chair configuration and the two C-C bonds on opposite sides of each hexagon are perpendicular to the tube axis. In the zig-zag nanotubes the terminal carbon atoms form zig-zag shape, and the two C-C bonds in opposite sides of the hexagon are parallel to the tube axis. In chiral nanotubes, these C-C bonds will be at an angle other than 0° and 90° with respect to the tube axis. A schematic representation of these structures is given in Figure 3.

Even though graphite is a very good electrical conductor, the conductivity of nanotubes, as mentioned before, depends on its structure. This is due to the confinement of the electrons around the circumference of the CNT compared to the planar structure of graphite. As a result of this, each band of graphene splits into several subbands. Depending upon the band gap, CNTs may be classified as three types. The first type is the metallic nanotubes and all the armchair nanotubes (m=n) are metallic in nature with very low band gap. The second type is the CNTs with small band gap (m-n=3i, i = 0) and in these nanotubes, the band gap arises due to the curvature effects and the band gap varies by $1/d_t^2$ where d_t is the diameter of the nanotubes. The large band gap CNTs (band gap of ~1eV) are semiconductors (m-n 6=3i) [40-41]. Since the electrons in the nanotube have only one-dimensional motion along the tube axis which results in reduced scattering, it leads to high current densities of the order of 10^9 A/cm^2 in metallic SWNTs, which is higher than metals like aluminum or copper [42]. Due to the unique electrical properties, SWNTs are explored for applications in a variety of fields such as biosensors, nanoactuators, FETs, logic gates, molecular electronics, supercapacitors and fuel cells.

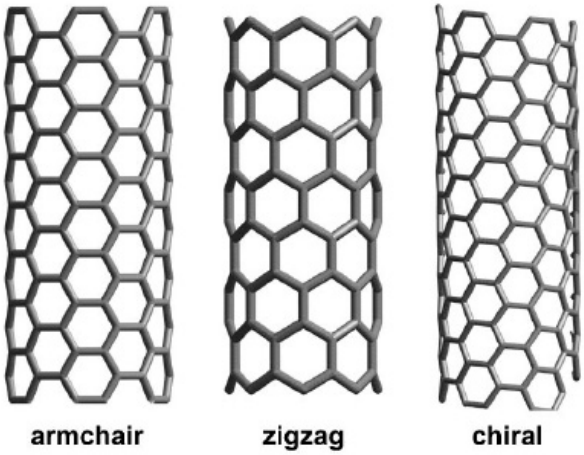

Figure 3. A schematic representation of armchair, zigzag and chiral nanotubes.

1.3 Monolayers

Electrochemistry, which among other things deals with the study of various processes at the electrode / electrolyte interface is a versatile area, which links different scientific disciplines such as chemistry, physics, biology and materials science. The electron transfer phenomenon occurring at the interface can be modeled to simulate the biological electron transfer processes. The behavior of electrode | electrolyte interface can be controlled and regulated by the adsorbed species on the surface of the electrode. The orientation and chemical nature of the adsorbed species on the metal electrodes are important since it affects the heterogeneous electron transfer events. The interaction of these species with the metal electrodes may be merely electrostatic, for example in the case of adsorption of anions or cations on a surface of opposite charge, or charge-dipole in nature as in the case of adsorption of amines, thiourea etc., or due to the formation of covalent bond as in the case of self-assembled monolayers.

Broadly, there are two methods of preparing the monolayer on the surfaces namely, the Langmuir-Blodgett method and molecular self-assembly method. The first method is commonly known as L-B technique that consists of transferring the molecules to a substrate by compression at the air-water interface [43]. The orientation of the transferred monolayer depends on the wetting properties of the substrate. Multilayers can also be prepared using this technique by successive dipping of the substrate at the interface. The other method of molecular self-assembly is based on the spontaneous adsorption of certain organic molecules on specific substrates to yield a structurally well defined, ordered monolayer [44]. Such organized molecular films exhibit several interesting properties and have potential applications in a variety of fields.

Adsorption of organic molecules with terminal thiol groups on noble metals such as gold, silver and copper attracted the attention of many researchers owing to their tendency to form a well ordered, oriented and highly dense monolayer on their surfaces. This technique is mainly used to modify the surface properties thereby finding potential applications in the field of sensors.

Controlled orientation of the biomolecules such as proteins onto the surfaces is necessary for the construction of highly reproducible biosensor. Many techniques such as electrostatic, covalent, and entrapment have been employed to immobilize the biomolecules onto the surfaces have been employed to obtain the reproducible results. Functionalized self-assembled monolayers on gold act as an effective surface for the controlled immobilization of biomolecules.

1.3.1 Self-Assembled Monolayer (SAM)

Self-assembled monolayers are molecular assemblies of ultrathin organic films of few nanometers thickness, which are formed by the spontaneous chemisorption of organic molecules onto an appropriate substrate when it is immersed into a dilute solution containing organic molecules dissolved in an organic solvent. The ideal picture of an organic monolayer consists of molecules with the head and tail groups oriented perfectly on a smooth substrate.

1.3.2 Monolayer Formation

The process of thiol SAM formation on gold surface is quite simple. A very clean, fresh gold substrate is immersed into a dilute solution containing thiol molecules dissolved in a solvent with immersion time varying from several minutes to days. This results in the formation of a close packed, highly ordered and oriented monolayer. This simple procedure has been used to produce diverse structures including the commonly used thiols with different terminal groups, aromatic thiol monolayers, attached polymers, attached pendent groups, lipids, proteins, peptides etc. There are several factors such as the substrate morphology, cleanliness of the substrate, purity of thiol, solvent used for adsorption, concentration of thiol and deposition time.

Most of the work on SAM formation has been performed on either evaporated or sputtered gold films on cleaved mica or single crystal silicon or glass under special conditions. The prepared gold substrates exhibit predominantly (111) crystal face [45-47] under certain appropriate conditions. Simple crystalline substrate containing a well defined

crystal face is preferred for many surface analytical methods such as electron diffraction, scanning tunneling microscopy etc., though it is not essential to obtain pinhole free SAMs.

The substrate cleanliness is very essential to produce a highly ordered and well-oriented monolayer. The very strong affinity of sulphur to gold ensures the displacement of weakly physisorbed materials from the substrate during the process of self-assembly [48]. There are several procedures such as strong heating of the substrate, immersion of the sample in strong oxidizing agents, exposure of the substrate to argon or oxygen plasma, ozone or UV radiations and electrochemical cycling in dilute acid solution, that are usually employed to clean the substrates before monolayer formation. ***"Piranha"*** solution, which is a mixture of concentrated sulphuric acid and 30% hydrogen peroxide in a 3:1 ratio, is a very common oxidizing agent to clean the Au substrate. The gold substrates are completely wetted by water after exposure to this kind of oxidizing agent. Since the wetting properties of bare gold samples are a sensitive test to the presence of organic contaminants, any partial dewetting of the gold surface by water indicates an incomplete cleaning. Prolonged exposure of the substrate to these kinds of oxidizing agents leads to the formation of a partial layer of gold oxide on the surface.

Although several commonly used organic solvents such as tetrahydrofuran (THF), n-hexane and acetonitrile are used for the preparation of SAMs, it is ethanol that has been mostly preferred and extensively used solvent due to its low toxicity, faint odour and availability in pure form. The concentration of the thiol molecules and the immersion time of the substrate play a very important role in the self-assembly process and thereby in the formation of monolayer. Typically, the concentration of the thiol used is in millimolar (mM) levels for SAM preparation.

1.3.3 Nature of Bonding Present in the Monolayer

The nature of bonding between the alkanethiol molecules and gold substrate is still a matter of considerable research. Both the alkanethiols and disulphides adsorb onto gold substrate to form the same thiolate (RS^-) species [49-50]. The reaction of dialkyldisulphides with gold is an oxidative addition reaction, which is given as follows.

$$RS - SR + Au^0_n \rightarrow 2\ R{-}S^-{-}Au^+ + Au^0_{n-2}$$

In the case of alkanethiol, the reaction may be considered as an oxidative addition of the thiol (S-H) to the gold surface, followed by a reductive elimination of hydrogen. When a clean gold surface is used for the monolayer preparation, the proton may probably end as a H_2 molecule. The chemical reaction occurs in this case is expressed as follows;

$$R–S–H + Au^{0}_{n} \rightarrow R– S^{-}–Au^{+} + Au^{0}_{n-1} + ½\ H_2$$

The combination of hydrogen atoms at the gold surface to produce H_2 molecule is an important exothermic step in the overall chemisorption energy involved in the process of self-assembly. During the chemisorption process, the thiolate species has been formed, as can be seen from the equation represented above. The bonding of thiolate group to the gold surface is very strong and the bond strength is approximately 40 kcal/mol. Figure 4 shows the steps involved in the process of self-assembly of alkanethiol molecules on gold surface.

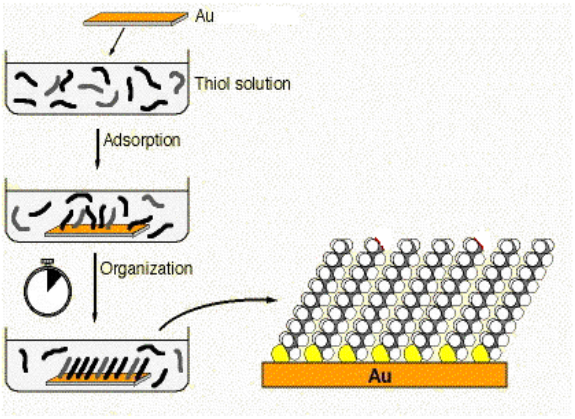

Figure 4. Self-assembly of alkanethiol molecules on gold substrate.

1.4 Biosensors

The process of attachment of biomolecules to the surface is called immobilization. The properties of proteins on the surfaces depend on the immobilization technique. Immobilization of proteins directly on the metal surfaces produces irreproducible results, as protein can attain any orientation on the surface. To obtain the reproducible results, studies have been carried out on modified functional surfaces, such as self-assembled monolayers, polymers, zeolites etc., [51-54]. Amongst all these, self-assembled monolayers offers particular advantage of immobilizing the proteins on the surface to control the precise orientation of biomolecules, which in turn helps in obtaining the reproducible results.

A biosensor is a self-contained integrated device which is capable of providing specific quantitative or semi-quantitative analytical information using a biological recognition element (biological receptor, selector) which is combined with a transducing (detecting) element.

A biosensor consists of two elements

1) (Bio) selector: The selector recognizes the analyte and reacts or binds to it.

2) Transducer: The transducer is the detector, monitoring the chemical or biochemical reaction initiated by the sample.

1.4.1 Selectors

The selectors of biosensors consist of biomolecules as biorecognition elements. The selectors determine the selectivity, so that only the compound which has to be measured provides the signal. The selection can be based on bioaffinity, in which the bioelement does not change the chemical structure of the analyte (e.g. an antibody), or biocatalysis, in which the bioelement catalyses a biochemical reaction of the analyte (e.g. an enzyme). Most biosensors described in literature use an enzyme as selecting element. The enzyme catalyses specifically a conversion of the analyte. Such a reaction has usually a high specificity and can be followed by measuring the increase in concentration of the product formed or the decrease of a co-substrate, which is consumed during the enzyme reaction. Cost of purification of enzymes is relatively cheap, because most enzymes can be isolated from micro organisms, such as fungi or bacteria, which produce these enzymes in excess, naturally or after genetic manipulation.

Biosensors are highly selective and sensitive. Because of their high selectivity biosensors find applications in medicines, food industries, environmental control etc.,

Extensive work has been carried out using enzyme glucose oxidase for catalytic determination of glucose oxidation. The enzyme catalyses specifically a conversion of the analyte. Glucose, oxidized by the enzyme glucose oxidase, is an example of an enzymatically detectable metabolite. When selective enzymes are not available for the detection of an analyte, antibodies can serve as selecting element. Antibodies can bind to analytes very selectively. Biosensors based on monitoring antibody-antigen interaction, are termed as immunosensors.

1.4.2 Transducers

The transducer (detector) translates the recognition of the selector into an analogue electrical signal which can be digitized. Table 1 shows the different transducers. The choice of the detection method is not only determined by the sensitivity of the detection method, but also by the contaminants present in the matrix. Most biosensors used so far apply optical or electrochemical detection.

In this thesis we have used electrochemical method for electron transfer and electrocatalytic studies of proteins. An advantage of electrochemical detection (ECD) devices is that the sensitivity is high and the materials that are required are cheap, compared to optical detection devices. Disadvantages of ECD-based sensors are that their signal may drift and also unspecific reduction or oxidation of compounds present in the sample may occur.

Device	Output change
amperometric	Current
potentiometric	voltage (potential)
capacitance/impedance	Impedance
light absorption or scattering, refractive index	light intensity, color, emission
mass/density	Weight
calorimetric	Temperature

Table 1. Shows the different types of transducers.

Thus, ECD devices have high sensitivity but relatively low specificity. An alternative detection method is measuring optical changes. Fluorescent (optical) signals can be created by probes carrying fluorescent dyes, or by probes containing enzymes, catalysing reactions forming fluorescent products. The sensitivity of electrochemical and fluorescent detection is often comparable, but fluorescent measurements encounter less interference. However, the apparatus required is large and both the equipment and the fluorescent dyes or substrates are expensive. Breakthrough in electrochemical biosensor started in 1962.

Clark et al. introduced the first biosensor for glucose [55]. This enzyme biosensor was based on detecting the decrease of oxygen, which was the co-substrate for the conversion of glucose by the enzyme glucose oxidase. Later, considerable amount of work has been carried out on different biosensor using different principle of detection. Table 2 summarizes the different indicator used for the particular substrate.

Determinant	**Substrate**	**Enzyme**	**Indicator**
saccharides	glucose	glucose oxidase	O_2 H_2O_2
	Lactate	lactate oxidase	O_2 H_2O_2
alcohols	Ethanol	ethanol oxidase	O_2
acids	acetic acid	alcohol oxidase	O_2
	uric acid	urease	H_2O_2
amino acids	glutamate	glutamate dehyrogenase	NH_4^+
lipids	cholesterol	cholesterol oxidase	H_2O_2
antibiotics	pencillin	pencillinase	pH electrode
other substrates	Urea	urease	NH_4^+
	inorganic phosphorus	alkaline phosphate	H_2O_2

Table 2. Shows the different indicator used in biosensor.

Electrochemical biosensors may be distinguished as amperometric, potentiometric, field effect or conductivity sensors. Amperometric biosensors are based on the measurements of the current resulting from the oxidation or reduction of an electroactive species, by keeping a constant potential at the working electrode (Pt, Au, Carbon, etc.) with respect to a reference electrode. The resulting current is correlated to the bulk concentration of the electroactive substance or its reaction within the adjacent bio-catalytic layer.

Potentiometric biosensors involve the determination of the potential difference between an indicator and a reference electrode (or two reference electrodes separated by a permselective membrane) without significant current flow. The transducer may be an ion selective electrode as recognition element, e.g. pH electrodes, ion or gas electrodes. Due to their typical electrochemical features the response of both amperometric and potentiometric biosensors is never in equilibrium, but either steady state or transient response.

1.4.3 Immobilization

Enzyme-based electrodes combine the specificity of an enzyme for its substrate and simplicity and sensitivity of electrochemical devices. The success of an enzyme based biosensor relies on how well the enzyme bonds to the sensor surface and remains there during use. Immobilization between matrix and bioreceptor has been shown as the typical procedure for improving the enzyme stability and thus general biosensor performances. Since the development of the enzyme-based sensor for glucose, first described by Clark in 1962 [55], in which glucose oxidase was entrapped between two membranes, an extensive literature on methods of immobilization and related biosensor development has appeared. After that, research work has provided a large number of support material and method for immobilization, several of which have been extensively reviewed in literature [56-57]. Biological receptors, enzymes, antibodies, tissues with a high biological activity, can be immobilized in a thin layer at the transducer surface by using different methods. Taking into account the relative use and application, both the choice of the support material and the main method of immobilization can influence not only the activity and the half-life of a biotransformation but also the operational stability of the biosensor. There are different methods for immobilizing enzyme on support materials: simple adsorption, covalent binding, entrapment, encapsulation, cross-linking etc.,

1.4.3.1 Adsorption

The immobilization by adsorption is a less complex method, for it involves reversible surface interactions between enzyme and support material. The forces involved are mostly electrostatic, as van der Waals forces, ionic and hydrogen bonds, although sometimes hydrophobic or hydrophilic, bonding can become significant. These forces are weak, but sufficiently large in number to enable reasonable binding.

1.4.3.2 Covalent Binding

This method involves the formation of covalent bonds. Functional chemical groups belonging to amino acid residues on the surface of the enzyme, which are not essential for activity, may be attached covalently to chemically activated supports such as SAM, synthetic polymers etc. A number of amino acid groupings are suitable for participating in covalent bond formation. Those mainly involved are the amino group of lysine or argirine, the carboxyl group of aspartic and glutamic acid. Figure 5a shows the schematic representation of the covalent modification of proteins to the carboxyl terminated surfaces using 1-Ethyl-3-(3-dimethylaminopropyl)-carbodiimide (EDC) in presence of N-hydroxysuccinimide. Figure 5b shows the schematic representation of the covalent modification of proteins to the amine terminated surfaces using glutaraldehyde as a cross linker.

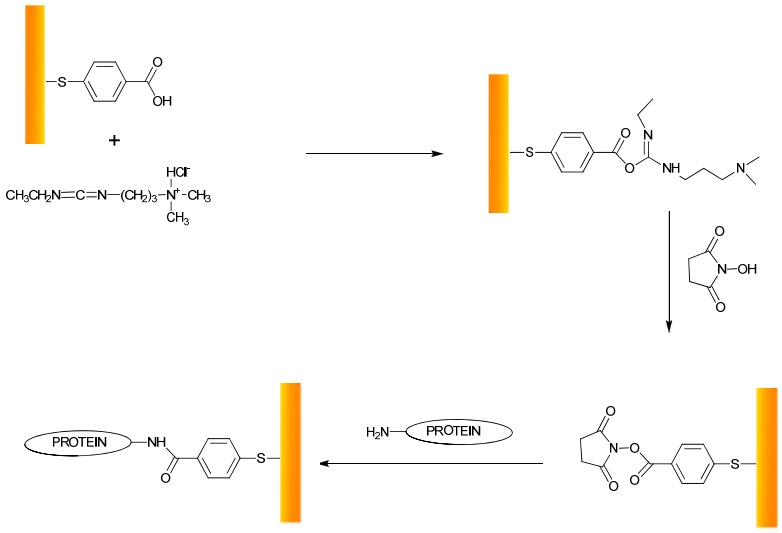

Figure 5a. Schematic of the covalent attachment of the protein to the carboxyl terminated surfaces

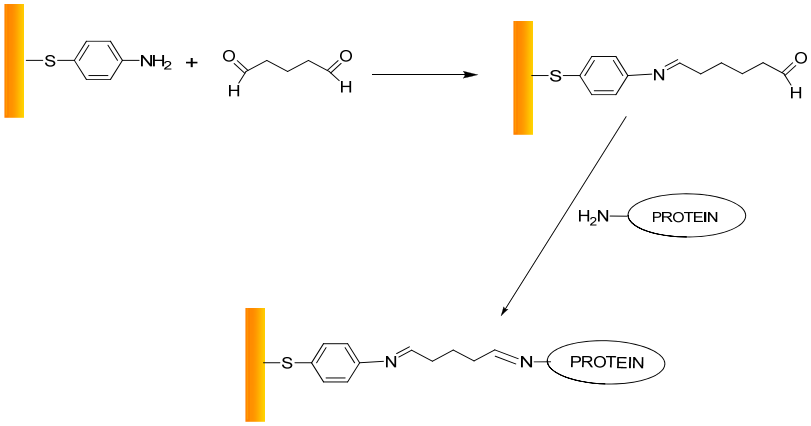

Figure 5b. Schematic representation of the covalent modification of proteins to the amine terminated surfaces.

1.4.3.3 Entrapment

Immobilization by entrapment differs from adsorption and covalent binding in that enzymes are free in solution, but restricted by the lattice structure of the entrapment system. It is possible to distinguish between three general methods:

1) Entrapment behind a membrane: a solution or suspension of enzymes, cells, a slice of tissue is confined by an analyte permeable membrane as a thin film covering the detector.
2) Entrapment of biological receptors within self assembled monolayers (SAMs) or bi-layer lipid membranes (BLMs).
3) Entrapment of biomolecules within a polymeric matrix membranes (such as polyacrylonitrile, agar gel, polyurethane, or polyvinyl-alcohol), redox gels, sol-gels with redox centres.

The most used technique is the entrapment in polymeric film (e.g. polypyrrole, Nafion) via casting or electropolymerisation, and in redox gel lattice. In the latter approach, gel porosity must be controlled to ensure that the structure is tight enough to prevent enzyme leakage, but at the same time to allow free movement of substrates and products. Inevitably, the support will act as a barrier to mass transfer with serious implications for reaction kinetics, but it has useful advantages, since harmful biological compounds are prevented from interaction with the immobilized biocatalyst. Additional improvement can be achieved combining several membranes or coatings, in order to extend the linear range (via reduction of the local substrate concentration) and to reject the potential interference of coexisting electroactive species.

1.5 Experimental Techniques and Their Working Principle

We have used a variety of experimental techniques in the course of our investigation and this section deals with those experimental techniques and their working principles. We have used several electrochemical, spectroscopic and microscopic techniques in this thesis work. Electrochemical techniques comprise of electrodeposition, cyclic voltammetry (CV), electrochemical impedance spectroscopy (EIS), stripping voltammetry, chronopotentiometry and Tafel plot analysis that have been extensively used in this study. The microscopic techniques such as scanning electron microscopy (SEM) and scanning tunneling microscopy (STM) have been carried out essentially to characterize the surface morphology and topography. Apart from these techniques, we have also used FTIR spectroscopy and diffraction studies in this work.

1.5.1 Cyclic Voltammetry (CV)

Cyclic voltammetry commonly known as "CV" is a very much popular and most extensively used electrochemical technique among the potential sweep techniques. The simplest of potential sweep techniques is linear sweep voltammetry (LSV), which involves sweeping the electrode potential between the limits E_1 and E_2 at a known sweep rate ν, before halting the potential sweep. In the case of cyclic voltammetry (CV) the waveform applied initially is same as LSV, but on reaching the potential E_2 the sweep is reversed usually at the same scan rate as the forward sweep instead of terminating the scan. Typical potential-time profile for CV is shown in Figure 6.

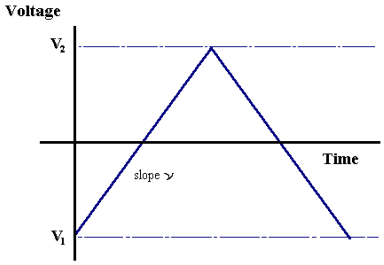

Figure 6. Potential-Time profile for cyclic voltammetry

Cyclic voltammetry concerns with the scanning of working electrode potential between the potential limits of V_1 and V_2 at a known scan rate ν, in both the forward and reverse direction and measuring the current of the electrochemical cell. The resultant current of the system involves the faradaic current due to the various electrochemical phenomenon occurring on the electrode surface such as electron transfer redox reactions and adsorption

processes in addition to the capacitive current due to the double layer charging at these potentials [58-59]. A plot of measured current as a function of applied potential is known as "cyclic voltammogram". It is an electrochemical spectrum indicating the potentials at which several processes occur can be obtained rapidly and from the dependence of current on the sweep rate, the involvement of coupled homogenous reactions and the process like adsorption can also be recognized. Apart from these, the kinetic parameters and the mechanism of different heterogeneous reactions occurring on the electrode surface can also be determined. The conventional experiments of recording voltammograms use a range of sweep rates varying from few mV/s to few hundred V/s for several values of V_1 and V_2. Usually there will be several peaks and by observing the characteristics of these peaks over the potential limits and as a function of scan rates, it is possible to determine and conclude how the processes represented by the peaks are related. By noting the difference between the first and subsequent cycles resulting in the cyclic voltammograms, detailed mechanistic information about the electrochemical reactions can be derived. Normally the shape of the cyclic voltammogram depends on the type of redox reactions. Figure 7 shows a typical cyclic voltammogram for a single electron redox process.

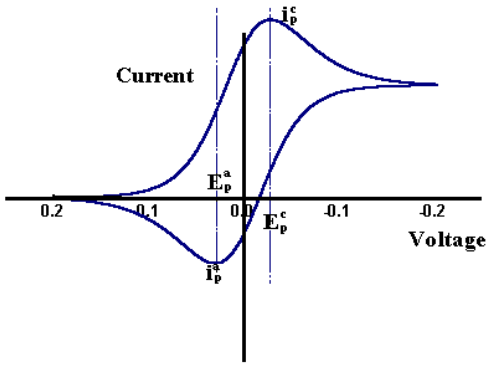

Figure 7. Cyclic voltammogram for a single electron reversible process

For a typical single electron reversible redox reaction of the type,

$$O + ne^- \rightleftharpoons R$$

the rate of charge transfer is always greater than the rate of mass transfer at all potentials and the redox reaction is under diffusion control. The ratio of concentrations of oxidant and reductant species of a reversible reaction is given by Nernst equation and a concentration gradient exists within the region near the electrode surface known as Nernst diffusion layer, where the concentration gradient of the electroactive species is linear. Also the Nernstian equilibrium is always maintained at the electrode surface and at all the potentials. The shape of current-potential profile for a one-electron reversible redox reaction as shown in Figure 7

can be understood in the following way. When the potential of the electrode is made more negative, the surface concentration of the reactant O decreases progressively, thereby increasing the concentration gradient is increased which results in increase in current. On reaching the electrode potential where O is reduced, the surface concentration of O decreases from its bulk value in order to satisfy the Nernst equation and the concentration gradient is setup. As a result a current proportional to the concentration gradient at the electrode surface flows. Due to diffusion of ions, the concentration gradient does not remain constant and it starts to decrease. At the same time, the electrode potential is also continuously changing leading to a further decrease of surface concentration of O until it effectively reaches zero concentration. Once the concentration of O reaches zero, the gradient decreases due to the accumulation of reduced species R, in the vicinity of the electrode surface (relaxation effect) and hence the current flow also decreases. Overall, this behavior gives rise to a peak shaped current-potential profile as shown in Figure 7. Using similar arguments used for the forward sweep, it can be shown that the current change on reverse sweep also exhibit a peak shaped response though of the opposite sign. On increasing the sweep rate, the concentration gradient as well as the current resulting from that also increases due to the shorter time scale of the experiment leading to less relaxation effect.

It can be seen from Figure 7 that the cyclic voltammogram for a reversible process shows a minimum charge associated with the anodic process of oxidation compared to that of the cathodic reduction process. This is because throughout the experiment, there is a concentration difference driving R away from the electrode surface resulting in diffusion of most of the product R to the bulk solution and cannot be reoxidised on the time scale of the experiment. The peak current density I_p of the cyclic voltammogram is related to various parameters by the following relationship.

$$I_p = -0.4463\ nF\ [nF/RT]^{1/2}\ c_o^{\infty}\ D^{1/2}\ \nu^{1/2}$$

where,

- I_p is the peak current density in A/cm^2
- n is the number of electrons involved in the redox reaction
- F is Faraday constant
- R is gas constant
- T is the absolute temperature
- C_o is the concentration of reactant O in mol/cm^3
- D is the diffusion coefficient in cm^2/s
- ν is the sweep rate in V/s

This equation is known as the Randles-Sevick equation and at a temperature of 25 ^{0}C this equation reduces to the form given as follows,

$$I_p = -(2.69 \times 10^5)\, n^{3/2}\, c_o^{\infty}\, D^{1/2}\, \nu^{1/2}$$

From the above equation, it can be noted that the peak current density of the reversible reaction is directly proportional to the concentration of the electroactive species, square root of the diffusion coefficient and also to the square root of the sweep rate. The sign of the current is negative because it is the current for cathodic reaction (as denoted by the convention followed).

A test of reversibility of the electrochemical system is to check whether a plot of I_p as a function of $\nu^{1/2}$ is both linear and passes through the origin or alternatively (I_p / $\nu^{1/2}$) is constant. If this is found to be true then further diagnostic tests, which are given below can be applied to verify the reversible nature of the given electrochemical system. For a reversible system the following are the diagnostic tests [8].

1. $\Delta E_p = | E_p^A - E_p^C | = 59/n$ mV
2. $| E_p - E_{p/2} | = 59/n$ mV
3. $| I_p^A / I_p^C | = 1$
4. $I_p \propto \nu^{1/2}$
5. E_p is independent of ν
6. At potentials beyond E_p, $I^{-2} \propto t$

Apart from the reversible system cyclic voltammetry can be used to find out the quasi-reversible and irreversible nature of the electrochemical system. There are also diagnostic tests for these systems to verify the quasi-reversibility and irreversibility of the given system.

Cyclic voltammetry technique has been extensively used in this work to study the electron transfer reactions and to measure the surface area of the electrodes in terms of roughness factor using conventional size macroelectrodes and disk/wire electrodes.

1.5.1.1 Determination of Real Surface Area of Metal Electrodes

A technique obtained by the slight modification of cyclic voltammetry (based on adsorption/stripping from solution) is very much useful in the determination of real surface area of the metal electrodes. This method is essentially based on hydrogen adsorption from solution in the potential region prior to massive hydrogen evolution and it has been established mainly with Pt, Rh and Ir electrodes [60-61]. The charge under the voltammetric peaks for hydrogen adsorption or desorption (after correcting for the double layer charging

current) is assumed to correspond to the adsorption of one hydrogen atom on each metal atom on the surface and is denoted by Q_H. The charge associated with a one to one M-H correspondence per unit surface area represented by, Q^S_H is calculated on the basis of distribution of the metal atoms at the surface. The true surface area in that case is given by,

$$\text{True surface area} = Q_H / Q^S_H$$

In the case of polycrystalline platinum, by assuming that the density of atoms on such a surface is 1.31×10^{15} cm^{-2}, the charge associated with the hydrogen adsorption is 210 μC cm^{-2} [59].

In some other cases, this method is based on the oxygen adsorption resulting in the formation and reduction of monolayer of oxide or hydroxide on the metal surface. Oxygen is assumed to be chemisorbed as a monoatomic layer prior to oxygen evolution with one to one correspondence with the surface metal atoms. In this case the charge associated with the formation or reduction of the oxide layer is given by,

$$Q_0 = 2 e N_A \Gamma_0 A$$

where N_A is the Avogadro number, Γ_0 is the surface concentration of atomic oxygen, which is assumed to be equal to N_M, the surface density of metal atoms and A is the area of the electrode. From the value of N_M per unit area, the reference charge value Q_0 can be determined.

The oxide/hydroxide stripping voltammetry is extensively used for gold electrodes. For polycrystalline gold, the charge corresponding to the desorption of monolayer of gold oxide is 390 μC cm^{-2}. The true surface area is calculated by measuring the charge of the modified electrodes in acidic or alkaline solution and dividing it by the actual charge value, from which the roughness factor can be determined.

$$\text{Roughness factor} = \text{True surface area} / \text{Geometric area}$$

Figure 8 shows the typical cyclic voltammogram of a gold electrode exhibiting the characteristic peaks of gold oxide formation and stripping in perchloric acid solution. The true surface area of gold electrode can be determined by measuring the charge under the gold oxide-stripping peak.

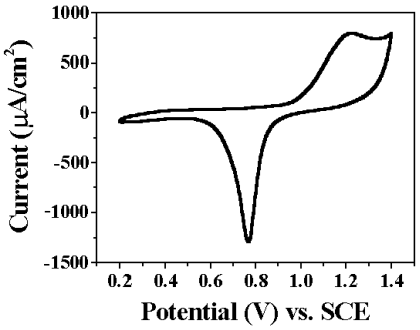

Figure 8. Cyclic voltammogram of a gold electrode in perchloric acid.

1.5.2 Electrochemical Impedance Spectroscopy (EIS)

This method comes under the category of ac techniques. In contrast to cyclic voltammetry, which is a dc technique, where the electrochemical system is perturbed far from equilibrium, this method involves the application of a very small perturbation close to the steady state equilibrium. The electrochemical impedance spectroscopy measurements involve essentially a small perturbation of the electrode potential from the equilibrium potential by the application of a sinusoidal signal with 5-10 mV peak-to-peak amplitude and measuring the response of the electrochemical system. Usually, the response to the perturbation, in terms of current differs in phase and amplitude from the applied signal. Figure 9 shows the sinusoidal signals of perturbation and response of the electrochemical system.

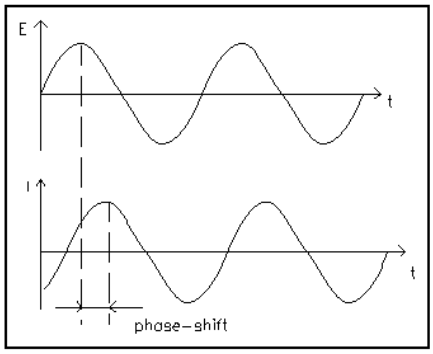

Figure 9. Sinusoidal signal of perturbation and response obtained in EIS.

The measurement of phase difference and amplitude (impedance) over a wide range of frequency is very much useful in the analysis of different electrode processes in relation to contributions from double layer charging, diffusion, kinetics, homogeneous and heterogeneous electron transfer reactions and coupled chemical and redox reactions etc. The impedance spectroscopy is extensively used in the study of corrosion, battery, membranes,

ionic solids, solid electrolytes, chemically modified electrodes and template deposited porous electrodes etc.

In many of the measurements involving the fast electron transfer reactions, the information has to be obtained at very short times, otherwise diffusion rather than the kinetics becomes the rate determining process. In such a case, the ac techniques are widely used to determine the rate constant for the fast redox reactions. Due to the small perturbation, the system becomes linear and the advantage lies in the ability to treat the response theoretically using the linearized current-potential characteristics. Since, the working region in this method is very close to the equilibrium, the detailed knowledge about the behaviour of current-voltage response over a large range of overpotential is not required. This simplifies the treatment of kinetics and diffusion equations. Using this method, the high precision measurements can be made because the response is indefinitely steady and therefore can be averaged over a long term. Usually, a comparison is made between the electrochemical cell and an equivalent circuit, which contains the combinations of resistances and capacitances that are assumed to behave like a cell. The aim of the impedance measurements is to interpret these equivalent circuits and the values determined using these circuits, in terms of the interfacial phenomena occurring at the electrode | solution interface. The impedance technique is frequently used for the evaluation of heterogeneous charge transfer parameters and to study the double layer structure.

1.5.2.1 Principles of AC Circuits

The electrochemical response of a cell to an ac perturbation can be understood by knowing the fundamental principles of ac circuits. If a sinusoidal signal of voltage $V = V_0 \sin \omega t$ is applied to an electrical circuit that contains a combination of resistors and capacitors, the response is a current, which is given by, $I = I_0 \sin (\omega t + \phi)$, where V_0 is the maximum amplitude, I_0 is the maximum current, ω is the angular frequency and ϕ is the phase angle between the perturbation and response. The proportionality factor between V and I is known as the impedance Z. In phasor terms the rotating vectors are separated in the polar diagram by the angle ϕ.

In the case of a pure resistor, R, the phase angle ϕ is zero. According to Ohm's law, $V = IR$, which leads to $I = V_0 \sin \omega t / R$. There is no phase difference between the potential and the current.

For a pure capacitor, C, the current I is given by,

$$I = C\, dV / dt$$

On substituting the value of V as $V_0 \sin \omega t$ and differentiating, we obtain,

$$I = \omega\, C\, V_0 \sin (\omega t + \pi/2)$$

$$I = V_0 \sin (\omega t + \pi/2) / X_C$$

where $X_C = (\omega\, C)^{-1}$ is known as the capacitive reactance.

Here we find that the phase angle is $\pi/2$, implying that the current leads the potential by 90^0 or $\pi/2$ in the case of a pure capacitor.

Similarly, for a circuit element containing a pure inductance, the potential leads the current by 90^0 or $\pi/2$.

1.5.2.2 Equivalent Circuit of an Electrochemical Cell

In general, an electrode | solution interface can be considered as an impedance to a small sinusoidal excitation. The impedance of such as a kind of electrochemical interface is a complex number, Z (ω) that can be expressed either in polar coordinates or in Cartesian coordinates, which are given as follows.

$$Z(\omega) = |Z|\, e^{j\phi}$$

$$Z(\omega) = Z'(\omega) + j\, Z''(\omega)$$

$$Z(\omega) = (\text{Re } Z)^2 + (\text{Im } Z)^2$$

where $Z'(\omega)$ and $Z''(\omega)$ are the real (Re Z) and imaginary (Im Z) parts of the impedance and the relationship between these quantities is given by,

$$|Z|^2 = (Z')^2 + (Z'')^2$$

The phase angle ϕ can be expressed as,

$$\phi = Arc \tan (\text{Im } Z / \text{Re } Z) \text{ or } Arc \tan (Z''(\omega) / Z'(\omega))$$

and $\quad \text{Re } Z \text{ or } Z'(\omega) = |Z| \cos \phi$

$$\text{Im } Z \text{ or } Z''(\omega) = |Z| \sin \phi$$

Hence the electrode | electrolyte interface of the electrochemical cell can be represented by a suitable equivalent circuit consists of resistors and capacitors that pass current with the same amplitude and the same phase angle under a given excitation. A typical equivalent circuit for an electrochemical system is shown in the following Figure 10.

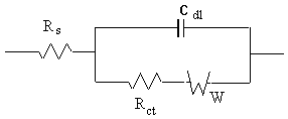

Figure 10. Randles equivalent circuit for an electrode reaction.

In Figure 10, an equivalent circuit popularly known as Randles equivalent circuit [62] for a diffusion controlled electron transfer reaction is shown with the double layer capacitance C_{dl}, the charge transfer resistance, R_{ct}, the Warburg impedance W and the solution resistance, R_s. The total current of the working electrode is obtained by the sum of distinct contributions from the faradaic current I_f and the double layer charging current I_c. The double layer capacitance arises from the charges stored at the interface between an electrode and its surrounding electrolyte. The charges in the electrode are separated from the charges of the bulk ions. In many cases, the double layer capacitance closely resembles a pure capacitance and hence it is represented by the element C_{dl} in the equivalent circuit. The faradaic impedance Z_f can be separated into two components namely, the charge transfer resistance, R_{ct} and the Warburg impedance, Z_W. The charge transfer resistance, R_{ct} denotes a resistance offered to the electron transfer process and Z_W also represents a kind of resistance to the mass transfer process because of diffusion. This impedance depends on the frequency of the perturbation in terms of the applied potential. At high frequencies, the Warburg impedance is small because the reactants do not have to diffuse very far. In contrast, at low frequencies, the diffusing reactants have to move very far, thereby increasing the Warburg impedance. The uncompensated solution resistance denoted by R_s exists between the working electrode and the reference electrode. In the equivalent circuit representation, the uncompensated solution resistance, R_s is inserted as a series element because all the current must pass through it. In contrast to R_s and C_{dl}, which are nearly ideal circuit elements, the components of faradaic impedance, Z_f namely the charge transfer resistance, R_{ct} and Warburg impedance, Z_W are not ideal because they change with the frequency ω.

For a planar diffusion, the value of R_{ct} can be expressed as,

$$R_{ct} = RT / nFI_0$$

where I_0 is the exchange current density.

The solution resistance R_s is given by the following expression,

$$R_s = x / \kappa A$$

where x is the distance of the capillary tip from the electrode

κ is the conductivity of the solution

A is the area of the electrode.

The relative values of R_{ct} and Z_W at a given frequency are the measure of the balance between kinetic and diffusion control. If the exchange current density I_0 is very large, then R_{ct} will tend to zero and its value will be too small to measure so that only the Warburg

impedance will be observed. On the other hand for a very sluggish electrochemical reaction, R_{ct} will be a dominant term and its value will be very high. The analysis of equivalent circuit and determination of the individual components of it was originated from a long procedure used in electrical engineering. It was first applied to electrochemical applications by Sluyters [63] and it is commonly known as ***Complex plane impedance analysis***. A full analysis of these series and parallel combination of elements known as the Randles equivalent circuit has two limiting cases. At low frequencies, as $\omega \rightarrow 0$, the real and imaginary parts of impedance are given by,

$$Z' = R_s + R_{ct} + \sigma\, \omega^{-1/2}$$

$$Z'' = \sigma\, \omega^{-1/2} + 2\, \sigma^2\, C_{dl}$$

where, $\sigma = (RT / \sqrt{2}\, n^2\, F^2\, A\, D^{1/2})\, \{\, 1 / C^{\infty}_{0} + 1 / C^{\infty}_{R}\}$

in which, D is the diffusion coefficient of the species in solution

A is the area of the electrode

C^{∞}_{0} and C^{∞}_{R} are the bulk concentrations of the oxidized and reduced species.

On rearranging these equations, we get,

$$Z'' = Z' - R_s - R_{ct} + 2\, \sigma^2\, C_{dl}$$

This is the equation of a straight line of unit slope and with an intercept on the real Z' axis given by, $R_s + R_{ct} - 2\, \sigma^2\, C_{dl}$

At high frequencies where the Warburg impedance is negligible in comparison to R_{ct}, the two components are represented by,

$$Z' = R_s + R_{ct} / (1 + \omega^2\, R_{ct}^2\, C_{dl}^2)$$

and $$Z'' = C_{dl}\, R_{ct}^2\, \omega / (1 + \omega^2\, R_{ct}^2\, C_{dl}^2)$$

Eliminating ω using these two equations gives,

$$(Z' - R_s - R_{ct}/2)^2 + (Z'')^2 = (R_{ct}/2)^2$$

which is the equation of a circle with center at $Z' = R_s + R_{ct}/2$ and a radius of $R_{ct}/2$.

A plot of the whole expression for Z' verses Z'' for a kinetically controlled reaction is shown in the Figure 11.

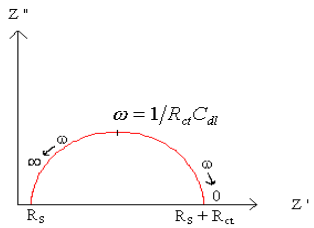

Figure 11. Cole-Cole plot.

The Cole-Cole plot of a charge transfer controlled reaction shows a semicircle and it is obtained by plotting the values of Z′ and Z″ at different frequencies. It is also known as the Nyquist plot. At infinite frequency, Z″ approaches zero as the capacitance in the equivalent circuit offers a very little impedance. At low frequencies, the impedance is purely resistive, because the reactance of C is very large. The solution resistance has the effect of translating the semicircle on the Z′ axis. R_s can be determined by reading out the real axis value at the high frequency intercept. C_{dl} can be obtained from the maximum value of Z″ in the semicircular region where $\omega = 1/R_{ct}C_{dl}$. The diameter of the semicircle provides the value of R_{ct}. Another way of representing the impedance data is by the Bode plot [13]. In this, both the logarithm of the modulus of impedance (log |Z|) and the phase angle ϕ are plotted in the y-axis against a common abscissa of frequency (in logarithmic scale). On such a plot a pure resistance is denoted by a horizontal line and a constant phase angle ϕ of 0^0, while a capacitor is a straight line of slope –1 and a constant phase angle ϕ of -90^0. The Bode plots for the Randles equivalent circuit without the Warburg impedance is shown in Figure 12.

Figure 12 shows two different kinds of representations of Bode plots. The first one is known as the Bode frequency plot and the other one is called as the Bode phase angle plot. The transition between the horizontal line and the sloping portion in the Bode frequency plot is called a corner and the frequency of intersection of lines extrapolating the straight-line sections is known as the corner frequency. The transitions between asymptotic values indicate the frequency regions where the ohmic and capacitive components have comparable values and neither of them is completely predominant. When the electrochemical system possesses more than one time constant, both the Bode plots and Cole-Cole plot exhibit the characteristic features.

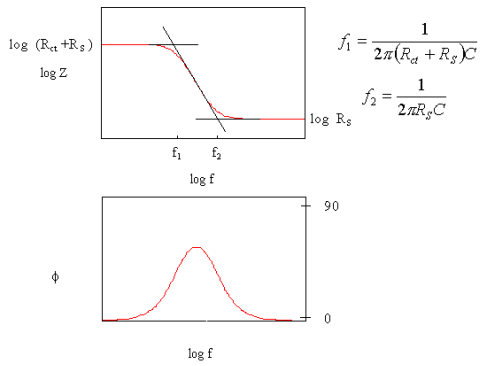

Figure 12. Bode plots.

1.5.2.3 Measurement of Impedance

The impedance measurements must be made over a wide range of frequency in order to attain the high frequency limit of the impedance equal to the electrolyte resistance. At high frequencies, the capacitive effect is attributed to a pure double layer capacitance. Normally the frequency range used for the measurement is from 100 mHz to 10 MHz, depending on the electrochemical system employed for the analysis. There are different types of methods used to measure the impedance of an electrochemical system namely, Wheatstone bridge, Analogue ac analyzer, Phase sensitive detection, Sine wave correlation, Frequency response analyzer and Fourier transform methods [58,59]. In our work, we have carried out the impedance measurements using a Perkin Elmer Model 5210 lock-in amplifier controlled by PowerSine software. In this case, Phase sensitive detection method [59] was employed to measure the impedance of an electrochemical cell above 5Hz using a Single-sine technique that provides the highest accuracy. Below 5Hz, the measurement of impedance was performed using a fast Fourier transform technique based on multi sine experiments that avoids any drift or change in the impedance value of the electrochemical system. The potential of the working electrode is held at a desired potential of interest using a potentiostat. A small amplitude of sinusoidal ac voltage with 5-10 mV peak-to-peak is applied to the cell from a lock-in amplifier. The current output from the cell has a phase difference with respect to the input voltage. The lock-in amplifier measures this phase difference and amplitude of the current response. Figure 13 shows the principle of working of a phase sensitive detector

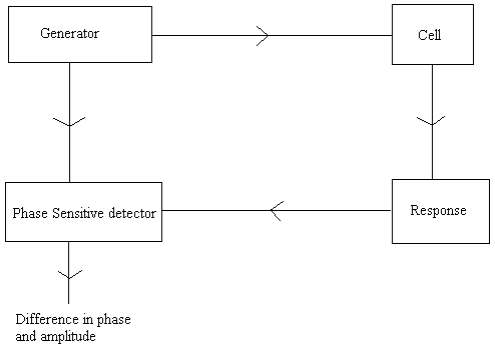

Figure 13. Schematic diagram of a Phase Sensitive Detector

The elements of an equivalent circuit model represent the various macroscopic processes involved in the transport of mass and charge in the electrochemical system. The dispersion relations with the frequency for most of the circuit elements are very simple. If the dispersion diagrams show distinct features that can be easily related to specific physical processes and can be defined to different sub-circuits of the equivalent circuit, then the

analysis becomes quite simple. However, if the time constants associated with different sub-circuits are relatively close to each other on the time axis or if the elements with fractional power dependence (<1) on frequency are present (For example, Warburg impedance or a Constant Phase Element (CPE)), then the dispersion curves become convoluted. In these cases, a more sophisticated method of analysis is required as the variation of one circuit element can affect a large part of frequency dispersion and hence affects the parameters of the other sub-circuits. To overcome this problem, Non-Linear Least Square Fit (NLLSF) technique is used, where all the parameters of the equivalent circuit are adjusted simultaneously. Using this technique, one can obtain the optimum fit to the measured dispersion data and a thorough treatment of this procedure to the electrochemical system was done by Bevington [63].

In this work, we have extensively used impedance spectroscopy to study the electron transfer reactions on the protein modified surfaces, to characterize the template electrodeposited materials. The measured impedance data were analyzed using the Boukamp's impedance software [64] by fitting to an appropriate equivalent circuit, which can significantly explain the processes occurring at the electrode | electrolyte interface. This software was written by Bernard A. Boukamp in Turbo Pascal (version 3.0) programming language. The impedance data were also analyzed using the ZsimpWin EIS data analysis software provided by Perkin Elmer (version 2.0).

1.5.3 Chronopotentiometry

In this type of experiment, the current flowing through the cell is instantaneously stepped from zero to some finite value and the potential of the working electrode is monitored as a function of time. Overall the rate of the reaction is fixed. This technique comes under the galvanostatic (constant current density) experiment. The plot of potential versus time is known as chronopotentiogram. Figure 14 shows a typical chronopotentiogram for a reversible system.

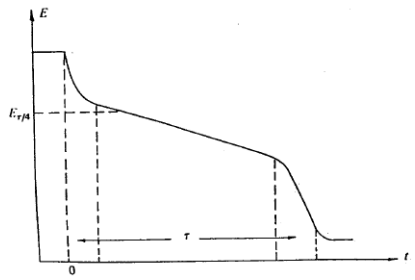

Figure 14. Schematic diagram of a chronopotentiogram for a reversible system

Consider a simple reaction, $O + ne^- \rightleftharpoons R$. As the current pulse is applied there is an initial fairly sharp decrease in the potential as the double layer capacitance is charged, until a potential at which the species O is reduced to R is reached. Then there is a slow decrease in the potential determined by the Nernst equation, until the surface concentration of O essentially reaches zero. The flux of O to the surface is then no longer sufficient to maintain the applied current and the electrode potential again falls sharply, until a further electrode process occurs. The dependence of current density on the transition time and the diffusion coefficient of the species in this case are given by Sand equation, which is represented as follows.

$$| I\tau^{1/2} | = n F D_0^{1/2} \pi^{1/2} C_0^{\infty} / 2$$

where τ is the transition time and D_0 is the diffusion coefficient of the species. Thus the product of $I\tau^{1/2}$ is independent of the applied current density and proportional to C_0^{∞}. This is used as a diagnostic test for diffusion controlled process. In our work, we have used chronopotentiometry to monitor the change of potential during the galvanostatic template free electrodeposition of gold.

1.5.4 Chronoamperometry

This method comes under the potential step experiment, where the potential of the working electrode is changed instantaneously and the current-time response is recorded. The plot of change of current with time at a constant potential is known as the chronoamperogram and the technique is called as the chronoamperometry. Figure 15 shows the typical potential step applied to an electrochemical system and its response in terms of current that is being recorded as a function of time.

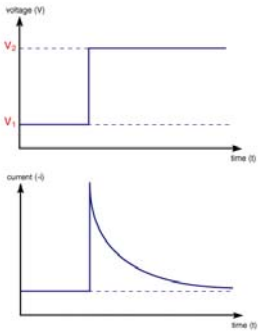

Figure 15. Schematic representation of potential step applied during chronoamperometric measurements and its response in terms of current as a function of time.

It can be seen from the figure that as soon as the potential is applied to an electrochemical system, there is a large flow of current due to the reaction occurring at the electrode surface. Initially the electrode surface is covered fully with the oxidant species and once the potential is applied to the electrode, the formation of reductant species occurs, which results in a large current flow. Further, this current decreases with time due to its dependence on concentration gradient. In our work, we have used this technique to evaluate various analytes.

1.5.4.1 Tafel Plot Analysis

Under steady state conditions, when the electron transfer process is irreversible, i.e. when current flows the electron transfer is insufficiently fast to maintain Nernstian equilibrium at the electrode surface, the kinetic data in such cases can be directly obtained from the steady state current-voltage measurements. The analysis is based on the Tafel equations, which are given as follows.

For a cathodic reaction,

$$\log |I| = \log I_0 - \alpha_C \, n \, F \, \eta \, / \, 2.303 \, RT$$

while for an anodic reaction,

$$\log |I| = \log I_0 + \alpha_A \, n \, F \, \eta \, / \, 2.303 \, RT$$

where I is the total current density, I_0 is the exchange current density, α_C and α_A are the respective cathodic and anodic Tafel slopes and η is the overpotential, which is defined as the deviation of applied potential from the equilibrium potential. Generally the Tafel approximation is used for $|\eta| \geq 70/n$ mV. The plot of log |I| versus η is known as the Tafel plot, from which the values of α_C, α_A and exchange current density (I_0) can be determined from the slopes and intercept respectively. The Tafel plot analysis is extensively used in the corrosion studies and catalysis especially for hydrogen evolving cathodes. In our work we have used Tafel plot analysis to study the hydrogen evolution reaction, methanol and ethanol oxidation reactions on the porous Au NP modified surfaces for evaluating it as a cathode in catalysis and understand the mechanism.

1.5.5 X-Ray Diffraction

X-ray diffraction (XRD) is a non-destructive technique for the qualitative and quantitative analysis of the crystalline materials, in form of either powder or solid. Basically XRD is obtained as the "reflection" of an X-ray beam from a family of parallel and equally spaced

atomic planes, on the basis of Bragg's law [65]. Diffraction occurs as the waves interact with a regular structure whose repeat distance is about the same as the wavelength.

In 1912, W.L. Bragg recognized that when certain geometric requirements are met, X-rays scattered from a crystalline solid could constructively interfere to produce a diffracted beam and has given a relationship based on the several factors known as the Bragg's law. The schematic representation of this law is shown in the following Figure 16.

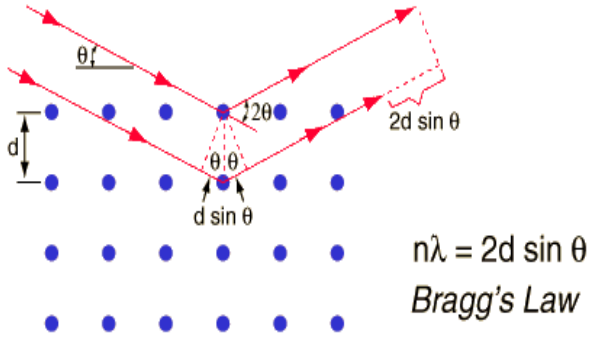

Figure 16. Schematic representation of Bragg's law

When a monochromatic X-ray beam of wavelength λ is incident on lattice planes with an angle θ, the diffraction occurs if the path of rays reflected by successive planes (with a distance 'd') is a multiple of the wavelength. Then it is possible to analyze the 'd' spacing of a crystal (or a powder) by measuring the first-order angles of diffraction, using the formula,

$$d = n \lambda / 2 \sin \theta$$

where, n is an integer, λ is the wavelength of X-rays in angstroms, d is the interatomic spacing in angstroms and θ is the diffraction angle in degrees. The wavelength of X-ray used for the analysis is 1.54 Å. X-rays with wavelength on the order of lattice spacing are elastically scattered (diffracted) from the atomic planes in a crystalline material yielding the diffraction peaks. The plot of intensity of X-ray with the diffraction angle (2θ) is known as the diffractogram. The qualitative analysis of the diffractogram obtained from the specimen can be done by comparing with a huge number of diffraction patterns available in the official database. Single phases and/or mixtures of phases can be analyzed with the programs available today. X-ray diffraction technique is widely used to identify the unknown crystalline phase, determine the residual stress, microstrain, preferred orientation and crystallite size or grain size and also in structural analysis of the specimen. Apart from this, XRD can also be used in the study of thin films to investigate the properties of the multilayer, by keeping the incident beam at very low angles thereby minimizing the interference due to

the substrate, as the same way reflectometry can be performed. In our studies, we have used surface XRD essentially to investigate the gold nanoparticle modified surface.

1.5.6 Scanning Electron Microscopy (SEM) and Transmission Electron Microscopy (TEM)

SEM comes under the category of electron microscopes, which were developed due to the limitations associated with the light microscopes such as the magnification and resolution. The electron microscopes are scientific instruments that use a beam of highly energetic electrons to image the specimen on a very fine scale and to gain information on its structure and composition. The analysis of images obtained from the electron microscope can provide information on the topography, morphology, composition and the crystallographic orientation of the sample. There are two kinds of electron microscopes namely Transmission electron microscope (TEM) and Scanning electron microscope (SEM) that are commonly used in the surface science. In our work, we have used SEM to characterize the surface morphology of the electrodeposited materials.

The first Scanning electron microscope (SEM) was introduced in the year 1942 to study the structural aspects of the surface on a very fine scale. SEM uses the electron beam rather than light to form an image. The electromagnets are used to bend the electron beam to produce the image on a screen. By using the electromagnets, we can have more control over the magnification and the use of electron beam provides a greater clarity in the image produced. There are many advantages of using the SEM instead of a light microscope. The SEM has a large depth of field, which allows a large amount of the sample to be in focus at one time. The SEM also produces images of high resolution, which means that closely spaced features can be examined at a very high magnification. The combination of higher magnification, larger depth of focus, greater resolution, and ease of sample preparation makes the SEM one of the most extensively used instruments in research areas today. A beam of electrons is generated from the electron gun using tungsten tip located at the top of the column. This beam is attracted through the anode, condensed by a magnetic lens and focused as a very fine point on the sample by the objective lens. The scan coils are energized (by varying the voltage produced by the scan generator) and create a magnetic field, which deflects the beam back and forth in a controlled pattern. Once the beam hits the sample surface there are many possibilities that can occur by the interaction of electron beam with the surface, which are shown in the Figure 17. As for as the SEM is concerned, when the electron beam hits the sample surface, the secondary electrons produced from the sample are

collected by the secondary electron detector or the backscatter detector, which can be converted into a signal resulting in an image in the viewing screen. The image obtained corresponds to the surface topography of the sample. When a SEM is used, the column must always be in a vacuum. This avoids the problem of interaction of electron beam with the other gaseous molecules, which would result in the lower contrast images. A very important point in the study of SEM is that the sample should be conductive and for this reason a thin film of gold is coated over the sample surface using sputtering technique before the process of imaging. In our work, we have used SEM to study the structural morphology of the template free electrodeposited materials and their characterization.

Transmission electron microscopy (TEM) is a microscopy technique where by a beam of electrons is transmitted through an ultra thin specimen, interacting with the specimen as it passes through. An image is formed from the interaction of the electrons transmitted through the specimen; the image is magnified and focused onto an imaging device, such as a fluorescent screen, on a layer of photographic film, or to be detected by a sensor such as a CCD camera. TEMs are capable of imaging at a significantly higher resolution than light microscopes, owing to the small de Broglie wavelength of electrons. This enables the instrument's user to examine fine detail—even as small as a single column of atoms, which is tens of thousands times smaller than the smallest resolvable object in a light microscope. TEM forms a major analysis method in a range of scientific fields, in both physical and biological sciences. In our studies TEM has been used to characterize gold nanoparticles.

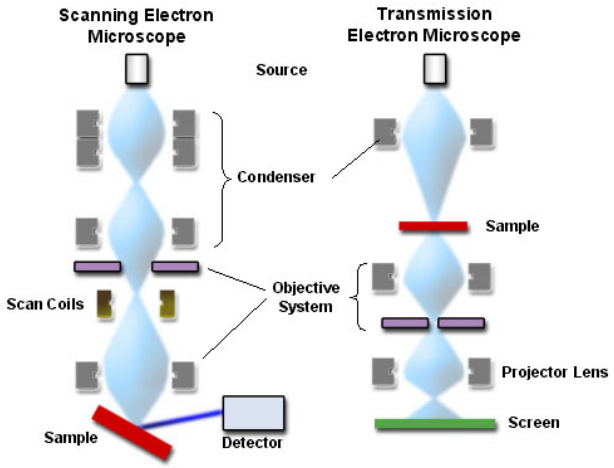

Figure 17. Schematic representation of SEM and TEM

1.5.7 Scanning Tunneling Microscopy (STM)

The Scanning Tunneling Microscopy (STM) [66] is a versatile tool to obtain the topographic images of smooth conductive surfaces in the area of surface science. The instrument scanning tunneling microscope was invented by Gerd Binnig and Heinrich Rohrer [67] at the IBM research institute, Zurich in the year 1982 for which they obtained the Nobel prize in 1985. It can be used in the investigation of very small areas of surfaces in the order of nanometers with extremely high level of precision. It also has the advantage of studying atomically smooth conducting surfaces in a variety of environments like ultra high vacuum (UHV), air, electrolytic media etc. In a typical STM experiment an atomically sharp metallic tip made up of either Pt/Ir, Pt/Rh, Pt or W is brought very close to the surface with the separation of the order of few angstroms between them. The movement of the tip in all the three direction is carried out with the help of piezoelectric crystals. Application of a small potential difference (~0.1V) between the sample surface and the tip leads to the flow of tunneling current in the order of pA to nA [68]. This tunneling is due to the fact that the electron wave functions of the tip and the sample overlap. The tunneling current is of the form $I_t \approx V\, e^{-kd}$ where I_t is the tunneling current, V is the bias voltage, *k* is a constant that includes the work function of the material and *d* is the spacing between the lowest atom on the tip and the highest atom on the sample. The exponential dependence of the tunneling current on the tip-to-sample spacing makes it possible to use this current in a feedback loop to control the motion of the tip precisely using a piezoelectric scanner. In response to an applied voltage, the scanner moves the tip over an area of the sample in a raster pattern and the feedback loop causes the tip to track the sample surface with sub-angstrom precision. The coordinates of the tip's path can then be transformed into a map of the surface topography. In fact, the STM image at atomic resolution corresponds to a contour map of the local density of states (LDOS) of atoms on a conducting sample. The tunneling current is very much sensitive to the distance between the tip and sample. This current decreases about one order of magnitude per 1Å of the electrical gap width, which results in an accuracy of the order of 0.1Å that can be achieved using STM. This extreme sensitivity of the STM means that the features, which are of atomic dimensions, can be imaged precisely provided the distance between the tip and the sample is accurately controlled. STM can be operated either in constant current mode or in constant height mode. In the constant current mode of operation, the tip is scanned over the sample surface in such a way that the gap separation is always maintained constant at a reference value, by the application of a feedback voltage to the inner piezo. The feedback voltage needed for

maintaining the tunneling current constant is a measure of the surface topographical image. For constant current mode, the feedback control unit plays a very important role. The feedback control unit compares the actual tunneling current with the user specified reference current. When the measured current is very large, the feedback control unit generates a voltage, which is applied to the piezo tube scanner to pull the tip back from the sample and vice versa. The piezo tube expands linearly with the applied voltage, which is directly proportional to the changes in the vertical tip position. In the constant height mode the tip is scanned over the sample in the same plane by keeping the gap separation constant, resulting in the variation of tip-sample separation depending upon the surface, which in turn changes the tunneling current ultimately. Figure 18 shows the schematic diagram of the working principle of STM. In our work, we have carried out STM studies extensively on the modified surfaces using a home built instrument and also commercial instrument Molecualar Imaging (Agilent, USA) [69-70].

1.5.8 Atomic Force Microscopy (AFM)

STM had a drawback that it can be used only for conducting surfaces. To overcome this, in 1985, Binning et al. developed AFM to measure ultra-small forces (< 1 μN) between the AFM tip and sample surface [71]. AFM does not require conducting substrate unlike STM. In atomic force microscopy image is created by scanning the surface of a sample with a sharp tip and measuring some highly localized tip-sample interaction as a function of position.

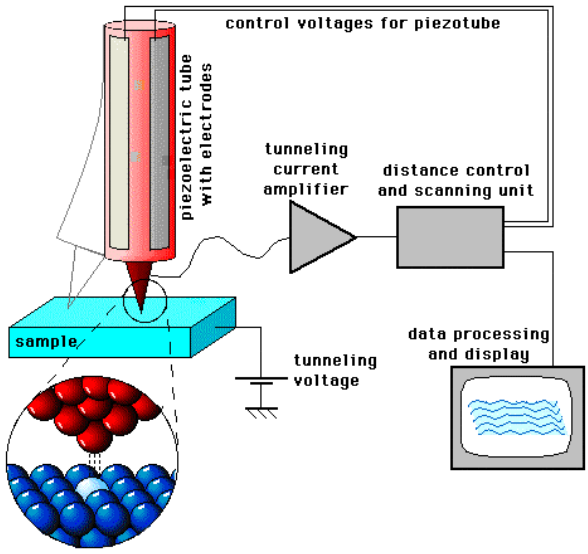

Figure 18. Schematic diagram of working principle of a STM

Figure 19 shows the picture of a scanning tunneling microscope that has been fabricated in our laboratory and extensively used for the study modified surfaces in this work.

Figure 19. Picture of the STM built in Raman Research Institute (RRI)

In AFM, the force between the tip and the sample is measured as a function of position. AFM cantilevers and tips are usually made up of silicon or silicon nitride as it is easy to microfabricate these materials. The force between the tip and the sample is calculated from the deflection of cantilever that occurs between due to the tip-sample interaction. The deflection in the cantilever is given by Hooke's law, $F = -K_cZ$, where F is the force between the tip and sample, K_c is the stiffness of cantilever and Z is the cantilever deflection. The deflection in cantilever is detected using an optical beam deflection method, where a laser beam is reflected from the back of the cantilever onto a split photodiode detector. The sub-angstrom deflections can be detected and, therefore, forces of picoNewton can be measured. The schematic diagram of AFM has been shown in the Figure 20.

1.5.8.1 Contact Mode

In contact mode AFM the tip is in contact with the sample. The interaction forces between the tip and sample causes the cantilever to deflect quasi-statically according to Hook's law and this deflection is directly measured. A feedback loop directly monitors the force between the tip and the sample by adjusting the cantilever-sample distance. The Z-position of the cantilever attached to the piezo is changed to keep constant distance between the tip and sample. Usually in the contact mode, the tip is very close to the sample surface and the interaction between them is due to repulsive forces.

1.5.8.2 Non-Contact Mode

In non-contact mode AFM, attractive forces which are of long range are used to monitor the tip-sample interaction. These attractive forces are weaker than the repulsive forces detected in

the contact mode and hence different methods are required to utilize them. In the non-contact mode AFM, the cantilever is intentionally excited by an electrical oscillator. As the cantilever approaches the sample surface, the tip sample interaction reduces the amplitude of cantilever oscillation. The amplitude of oscillation is kept constant at a fixed cantilever-sample distance. The sample is scanned at constant amplitude using a feedback loop. The change in the Z-position of the cantilever to keep the amplitude at the fixed value gives the topography information. In addition to this, the phase difference between the oscillation of cantilever and external electrical oscillator can be used to differentiate areas on the sample surface with different stiffness, adhesion and viscoelasticity.

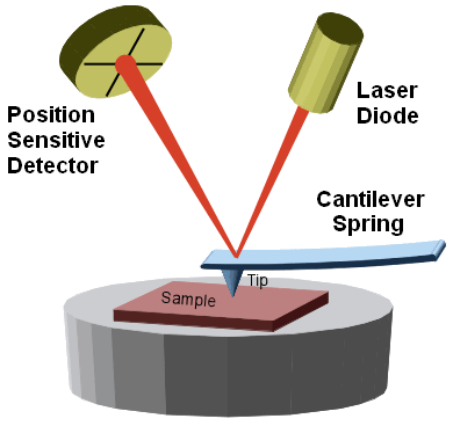

Figure 20. Schematic diagram of AFM.

1.6 References

[1] U. Kreibig, M. Vollmer, *Optical Properties of Metal Clusters; Springer:* Berlin, **1995**.

[2] A. N. Shipway, E. Katz, I. Willner, *Chem. Phys. Chem* **2000**, *1*, 18.

[3] D. M. Adams, L. Brus, C. E. D. Chidsey, S. Creager, C. Creutz, C. R. Kagan, P. V. Kamat, M. Lieberman, S. Lindsay, R. A. Marcus, R. M. Metzger, M. E. Michel-Beyerle, J. R. Miller, M. D. Newton, D. R. Rolison, O. Sankey, K. S. Schanze, J. Yardley, X. Zhu, *J. Phys. Chem. B* **2003**, *107*, 6668.

[4] M. -C. Daniel, D. Astruc, *Chem. Rev.* **2004**, *104*, 293.

[5] M. G. Warner, J. E. Hutchison, In *Synthesis, Functionalization and Surface Treatment of Nanoparticles*, Ed. by M. –I. Baraton, *American Scientific Publishers: California,* **2003**, 67.

[6] P. Atkins, J. D. Paula, *Physical Chemistry Oxford University Press*, **2002**, 908.

[7] A. Roucoux, J. Schulz, H. Patin, *Chem. Rev*. **2002**, *102*, 3757.

[8] D. Astruc, F. Lu, J. R. Aranzaes, *Angew. Chem. Int. Ed*. **2005**, *44* 7852.

[9] N. Pernicone, *Cattech*, **2003**, *7*, 196.

[10] G.A. Somorjai, Y.G. Borodko, *Catal. Lett*. **2001**, *76*, 1.

[11] M. Haruta, N. Yamada, T. Kobayashi, S. Iijima, *J. Catal*. **1989**, *115*, 301.

[12] R. Nishio, M. Sugiura, S. Kobayashi, *Org. Lett*. **2005**, *7*, 4831.

[13] B. Yoon, H. Kim, C.M. Wai, *Chem. Comm*. **2003**, 1040.

[14] I. P. Beletskaya, A. N. Kashin, A. E. Litvinov, V. S. Tyurin, P. M. Valetsky, G. van Koten, *Organometallics* **2006**, *25*, 154.

[15] M. Brust M. Walker, D. Bethell, D. J. Schriffin, R. Whyman. *J. Chem. Soc. Chem. Commun.* **1994**, 801.

[16] M. Brust, C. J. Kiely, *Colloids and Surfaces A-Physicochemical and Engineering Aspects* **2002**, *202*, 175

[17] E. Katz and I. Willner. *Angew. Chem. Int. Ed.*, 43:6042, 2004.

[18] A. C. Templeton, W. P. Wuelfing, R. W. Murray, *Acc. Chem. Res.* **2000**, *33*, 27.

[19] E. A. Hauser, J. E. Lynn, *Experiments in colloid Chemistry, McGrawHill, Newyork,* **1940**, 18.

[20] J. Turkevitch, *Gold Bulletin* **1985**, *18*, 86.

[21] H. Hirai, Y. Nakao, N. Toshima, *J. Macromol. Sci. Chem*. **1978**, *A12*, 1117.

[22] H. Hirai, *J. Macromol. Sci. Chem*. **1979**, *A13*, 633.

[23] H. Hirai, Y. Nakao, N. Toshima, *J. Macromol. Sci. Chem*. **1979**, *A13*, 727.

[24] C. Ducamp-Sanguesa, R. Herrera-Urbina, M. Figlarz, *J. Solid State Chem*. **1992**, *100*, 272.

[25] M. T. Reetz, W. Helbig, *J. Am. Chem. Soc.* **1994**, *116*, 7401.

[26] X. Liu, M. Atwater, J. Wang, Q. Huo, *Colloid Surface B* **2006,** *58,* 3.

[27] C. N. R. Rao, P. J. Thomas, G. U. Kulkarni, *Nanocrystals: Synthesis, Properties, and Applications, Springer,* **2007**, Chapter 1, 12-14.

[28] E. Katz, I. Willner, *Angew. Chem. Int. Ed.* **2004**, *43*, 6042.

[29] D. I. Gittins, D. Bethell, R. J. Nichols, D. J. Schriffin, *Adv. Mater.* **1999**, *11*, 737.

[30] W. Cheng, S. Dong, E. Wang, *Langmuir* **2002**, *18*, 9947.

[31] Vincent Rotello, *Nanoparticles: Building Blocks for Nanotechnology: Springer,* **2004.**

[32] S. Ijima *Nature* **1991**, *354*, 56.

[33] S. Ijima, T. Ichihashi, *Nature* **1993**, *363*, 603.

[34] D. S. Bethune, C. H. Kiang, M. S. de Vries, G. Gorman, R. Savoy, J. Vazquez, R. Beyers, *Nature* **1993**, *363*, 605.

[35] V. N. Popov, *Materias Sci. Engg. R* **2004**, *43*, 61.

[36] M. Terrones. *Annu. Rev. Mater. Res.* **2003**, *33*, 419.

[37] C. Journet, W. K. Maser, P. Bernier, A. Loiseau, M. L. de la Chapelle, S. Lefrant, P. Deniard, R. Lee, J. E. Fischer. *Nature*, **1997**, *388*, 756.

[38] A. Thess, R. Lee, P. Nikolaev, H. Dai, P. Petit, J. Robert, C. Xu, Y. H. Lee, S. G. Kim, A. G. Rinsler, D. T. Colbert, G. E. Scuseria, D. Tomanek, J. E. Fischer, R. E. Smalley, *Science* **1996**, *273*, 483.

[39] S. Mohanapriya, V. Lakshminarayanan. *Talanta* **2007**, *71*, 493.

[40] M. S. Dresselhaus, G. Dresselhaus, A. Jorio, *Annu. Rev. Mater. Res.* **2004**, *34*, 247.

[41] M. Ouyang, J. L. Huang, C. L. Cheung, C. M. Lieber, *Science*, **2001**, *292*, 702.

[42] P. Avouris, *Acc. Chem. Res.* **2002**, *35*, 1026.

[43] G. G. Roberts, *Langmuir-Blodgett films*, *Plenum Press, New York*, **1990**.

[44] A. Ulman, *Chem. Rev.* **1996**, *96*, 1533.

[45] Y. Golan, L. Margulis, I. Rubinstein, *Surf. Sci.* **1992**, *264*, 312.

[46] C. A. Widrig, C. Chung, M. D. Porter, *J. Electroanal. Chem.* **1991**, *310*, 335.

[47] S. D. Evans, K. E. Goppert-Bearducci, E. Urankar, L. J. Gerenser, A. Ulman, *Langmuir* **1991**, *7*, 2700.

[48] E. B. Troughton, C. D. Bain, G. M. Whitesides, R. G. Nuzo, D. L. Allara, M. D. Porter, *Langmuir* 1998, 4, 365.

[49] C. A. Widrig, C. Chung, M. D. Porter, *J. Electroanal. Chem.* **1991**, *310*, 335.

[50] H. A. Biebuyck, C. D. Bain, G. M. Whitesdies, *Langmuir* **1994**, *10*, 1825.

[51] S. Song, R. A. Clark, E. F. Bowden, *J. Phys. Chem*. **1993**, *97*, 6564.

[52] H. Liu, H. Yamamoto, J. Wei, D. H. Waldeck, *Langmuir* **2003**, *19*, 2378.

[53] K. Sirkar, A. Revzin, M. V. Pishko, *Anal. Chem.* **2000**, *72*, 2930.

[54] Z. Dai, S. Liu, H. Ju, *Electrochim. Acta* **2004**, *49*, 2139.

[55] J. Wang, Analytical Electrochemistry, wiley-VCH, 2006.

[56] J. Wang, *Chem. Rev.* **2008**, *108*, 814.

[57] T. Wink, S. J. van Zuilen, A. Bult, W. P. Bennekom, *Analyst* **1997**, *122*, 43R. [58] A. J. Bard, L. R. Faulkner, *Electrochemical Methods – Fundamentals and Applications*, John Wiley & Sons, New York, **1980**.

[59] *Southampton Electrochemistry Group Instrumental methods in Electrochemistry, Ellis Horwood Limited,* **1985**.

[60] S. Trasatti, O. A. Petrii, *Pure & Appl. Chem.* **1991**, *63*, 711.

[61] E. Yeager, J. O. M. Bockris, B. E. Conway, S. Sarangapani *Comprehensive Treatise of Electrochemistry*, *Plenum Press*, **1981**, *9*.

[62] J. E. B. Randles, *Disc. Faraday Trans Soc.* **1947**, *1*, 11.

[63] M. Sluyters-Rehbach, J. H. Sluyters, in *Electroanalytical Chemistry*, by A. J. Bard (Ed), Volume 4, Chapter 1, Marcel Dekker, New York, (1970).

[63] P. R. Bevington, in *Data Reduction and Error Analysis for the Physical Sciences*, McGraw-Hill, New York, **1969**.

[64] B. A. Boukamp, *Equivalent Circuit Software*, Perkin Elmer, Second edition.

[65] C. W. Bunn, *Chemical crystallography: An Introduction to Optical and X-ray methods*, *Second edition, Clarendon Press, Oxford*, **1961**.

[66] C. Julian Chen, *Introduction to Scanning Tunneling Microscope*, *Oxford University Press, New York*, **1993**.

[67] G. Binnig, H. Rohrer, C. Gerber, E. Weibel, *Appl. Phys. Lett.* **1982**, *40*, 178.

[68] C. Bai, *Scanning Tunneling Microscopy and its applications, Springer Series in Surface Science,* **1992**, *32*.

[69] V. Lakshminarayanan, *Curr. Sci.* **1998**, *74*, 413.

[70] M. Jayadevaiah, V. Lakshminarayanan, *Meas. Sci. Technol.*, **2004**, 15, N35.

[71] G. Binning, C. F. Quate, Ch. Gerber, *Phys. Rev. Lett.* **1986**, *56*, 930.